



Optimal Design of Capacitive Micro Cantilever Beam Accelerometer

Othman Sidek

Collaborative Microelectronic Design Excellence Centre
Universiti Sains Malaysia, Engineering Campus, 14300 Nibong Tebal
Sri Ampangan, Pulau Pinang, Malaysia
Tel: 60-3-599-5800 E-mail: othman@cedec.usm.my

Muhamad Azman Miskam

Collaborative Microelectronic Design Excellence Centre
Universiti Sains Malaysia, Engineering Campus, 14300 Nibong Tebal
Sri Ampangan, Pulau Pinang, Malaysia
Tel: 60-3-599-5856 E-mail: azman@cedec.usm.my

H.M.T. Khaleed

School of Mechanical Engineering
Universiti Sains Malaysia, Engineering Campus, 14300 Nibong Tebal
Sri Ampangan, Pulau Pinang, Malaysia
Tel: 60-3-599-6369 E-mail: khalid_tan@yahoo.com

Mohd Fauzi Alias

Collaborative Microelectronic Design Excellence Centre
Universiti Sains Malaysia, Engineering Campus, 14300 Nibong Tebal
Sri Ampangan, Pulau Pinang, Malaysia
Tel: 60-3-599-5856 E-mail: fauzi@cedec.usm.my

Shukri Korakkottil Kunhi Mohd

Collaborative Microelectronic Design Excellence Centre
Universiti Sains Malaysia, Engineering Campus, 14300 Nibong Tebal
Sri Ampangan, Pulau Pinang, Malaysia
Tel: 60-3-599-5962 E-mail: shukri@cedec.usm.my

Abstract

This study presents the behavior of a micro cantilever beam accelerometer under electrostatic actuation by using the analytical and numerical method. The objective of this study is to determine optimal design of capacitive micro cantilever beam accelerometer in term of reducing the beam deflection with respect to applied acceleration but keeping the distance between electrodes. The structure contains proof mass which is suspended between fixed rigid electrodes to provide differential capacitance measurements. ANSYS[®] is used for finite element analysis (FEA) modeling and simulation. The analytical modeling is done by using C programming. Three dimensional modeling is done for six different loading conditions in order to come out with the optimal design. The results obtained from both the analytical and finite element models are found to be in excellent agreement.

Keywords: Microelectromechanical system, Microaccelerometer, Inertial sensors, Micromachined sensors, Silicon sensors

1. Introduction

Recent scientific and technological advances in micro technologies have produced an increasing interest in the application of micromechanical freestanding structures (cantilevers, bridges and diaphragms) in many fields where advance performance, high sensitivity and reduce dimensions are required (Bianco et al., 2008). Cantilever beams are widely used as the basic components in micro-sensors, micro-switches and RF-MEMS as well as in experimental micromechanics for evaluating mechanical properties and the strength of materials (Ballestra et al., 2008).

Sensors and actuators are the two main categories of the microelectromechanical system (MEMS). A sensor is a device that measures information from a surrounding environment and provides an electrical output signal in response to the parameter it measures. An actuator is a device that converts an electrical signal into an action. It can create a force to manipulate itself, other mechanical devices or the surrounding environment to perform some useful function. A variety of different basic principles are used to implement MEMS actuators including electrostatic, piezoelectric, magnetic, magnetostrictive, bimetallic and shape-memory alloy. MEMS accelerometers can be fabricated by using bulk micromachining or surface micromachining. (Fricke and Obermier, 1993). The technology of MEMS enables the fabrication of tiny, mechanical structures from silicon wafers offering three characteristic features of technology, miniaturization multiplicity and microelectronics.

A MEMS capacitive-type sensor is basically an electrostatic transducer that depends on electrical energy in terms of constant voltage (voltage drive) or constant charge storage (current drive) to facilitate the monitoring of capacitance change due to an external mechanical excitation such as force, acoustical pressure or acceleration. Capacitive micro accelerometers have the combined advantages of high sensitivity, good dc response and noise performance, low-drift, low-temperature sensitivity and low-power dissipation. In many of the capacitive sensing accelerometers, the acceleration force (in terms of g) deflects the proof mass. Micro fabricated cantilever beams are widely used in MEMS capacitive-type sensors as the sensing element (Chowdhury et al., 2005). Vivek et al. (2006) proposed a design methodology for a micro machined single axis silicon capacitive accelerometer. This methodology will be able to reduce time and cost. Coventorware software is used to simulate finite element analysis and the Particle Swarm Optimization (PSO) technique is used as a tool for dimensions optimization. The limitation of the design is the die size i.e. minimum beam thickness is fixed at 40 μm and the thickness of the proof mass is fixed at 575 μm . Five different structures were analyzed and it was observed that to square the square proof mass with eight Beam Bridges was the optimal solution. Heng Yang et al. (2005) studied the design, fabrication and initial measurement of a cantilever beam pull-in accelerometer. They carried out analytical modeling and found that sensitivity and nonlinearity decreased with the increase of the driving torque and increased with the increase of the damping.

Substantial efforts have been made by many researchers to know the exact behavior of the cantilever beam when it has been subjected to force. Puersy and Reyntjensz (1998) characterized a miniature silicon micromachined capacitive accelerometer with a size of 500 x 500 μm^2 and fabricated using bulk micromachined technology. They found from static measurements that the measured sensitivity (z-direction) of the device is less than the expected value and the asymmetric suspension system causes considerable deviations from the ideal behavior. Thus, it is very important to know the deflection of the cantilever beam and to optimize the design of the beam-mass structure to achieve the required deformation. The necessity to compute the deflection of the cantilever and the freely suspended mass is to know the effect of deflection on the electrode which has been placed at the air gap. In the present study, a capacitive micro cantilever beam is simulated according to device dimensions taken from the literature. ANSYS software is used to simulate the model FEM and C programming is used to analytically determine the displacement of the proof mass according to different accelerations.

2. Methods

2.1 Mathematical modeling

The simplified model for the basic mechanical properties of the beam-mass structure is shown in Figure 1. In this model, the beam and the mass are considered to have a rectangular cross section. The length, thickness and width of the beam are a_1 , h_1 and b_1 respectively. The thickness and the width of the mass are h_2 and b_2 respectively. The length of the mass is $a_2 - a_1$. If the mass center is located at $x=L$ in the coordinate system,

$$L = \frac{1}{2}(a_1 + a_2) \quad (1)$$

The differential change of the capacitance due to the deflection of the proof mass can be used to estimate the sensitivity, resolution and non-linearity of the sensor. The deflection of the beams and the proof mass can be estimated by double integration or by the successive integration method. The dynamic behavior is analyzed by determining the natural frequency and the damping force. Assuming that the mass of the beam is negligible hence the proof mass is rigid i.e.

no bending takes place. Assuming the accelerometer is under acceleration, a , in the z -direction, the stress and displacement are caused by the acceleration.

2.1.1 Stress Analysis

The differential equation for region 1 (the beam region, in $0 < x < a_1$) is:

$$-EI_1 w_1''(x) = -m_o + F_o x \quad (2)$$

Where $I = \frac{1}{12} b_1 h_1^3$, $F_o = ma$ and $m = 2(L - a_1)h_2 b_2 \rho$. The differential equation for region 2 (the mass region in $a_1 < x < a_2$) is

$$-EI_2 w_2''(x) = -m_o + F_o x - \frac{I}{2} (x - a_1)^2 b_2 h_2 \rho a \quad (3)$$

When $w_1''(a_2) = 0$;

$$m_o = maL = F_o L \quad (4)$$

By substituting equation (4) into equation (1);

$$w_1''(x) = \frac{12(L-x)ma}{Eb_1 h_1^3} \quad (5)$$

The stress on the surface of the cantilever beam $\left(z = -\frac{h_1}{2}\right)$ is:

$$T_c(x) = \frac{6ma(L-x)}{b_1 h_1^2} \quad (6)$$

The maximum stress on the beam is at $x=0$ and the value is:

$$T_{cmax} = T_c(0) = \frac{6maL}{b_1 h_1^2} \quad (7)$$

2.1.2 Displacement

According to Equation (5), ($w_1(0) = w_1'(0) = (0)$), the slope of the beam is:

$$w_1'(x) = \frac{6ma(2L-x)x}{Eb_1 h_1^3} \quad (8)$$

The displacement of the beam is:

$$w_1(x) = \frac{2ma(3L-x)x^2}{Eb_1 h_1^3} \quad (9)$$

The maximum displacement of the beam is at $x=a_1$ and the value is:

$$w_1(a_1) = \frac{2ma(3L-a)a_1^2}{Eb_1 h_1^3} \quad (10)$$

The slope at that point is:

$$w_1'(a_1) = \frac{6ma(2L-a_1)a_1}{Eb_1 h_1^3} \quad (11)$$

As the mass is much thicker than the beam, the deflection of the mass is negligible. Therefore, the displacement in region 2 can be approximated by:

$$w_2(x) = w_1(a_1) + w_1'(a_1)(x - a_1) \quad (12)$$

According to Equations 10, 11 and 12, the displacement of the mass is:

$$w_2(x) = \frac{2ma}{Eb_1 h_1^3} [3(2L-a_1)x - (3L-2a_1)a_1] a_1 \quad (13)$$

The displacement at the mass center ($x=L$) is found to be:

$$w_2(L) = \frac{4ma}{Eb_1 h_1^3} (3L^2 - 3La_1 + a_1^2) a_1 \quad (14)$$

The maximum displacement is at the far end of the mass ($x=a_2=2L-a_1$) and can be expressed as:

$$w_{max} = \frac{2ma}{Eb_1 h_1^3} (12L^2 - 15La_1 + 5a_1^2) a_1 \quad (15)$$

The analytical simulation is done by using C programming and the system interface is shown in Figure 2.

2.2 Finite element analysis

The design models are modeled in ANSYS and divided into the required number of segments in order to obtain element continuity. The 2D model is meshed with 2D (quadrilateral) solid ELEMENT 42 and the same elements are extruded to 3D (hexahedra) solid ELEMENT 45. The beam is fixed at the left surface, the all degree of freedom have been constrained. and load has been applied at the middle node upper surface of rear end of the mass. The simulation assumes that the deflection of the electrodes is not considered and the mass is thicker than the beam hence the deflection of the mass is negligible.

PLANE42 is used for the 2-D modeling of solid structures (Figure 3). The element can be used either as a plane element (plane stress or plane strain) or as an axisymmetric element. The element is defined by four nodes having two degrees of freedom at each node: translations in the nodal x and y directions. The element has plasticity, creep, swelling, stress stiffening, large deflection, and large strain capabilities. The geometry, node locations, and the coordinate system for this element are shown in Figure 4. The element input data includes four nodes, a thickness (for the plane stress option only) and the orthotropic material properties. Orthotropic material directions correspond to the element coordinate directions. Pressures may be input as surface loads on the element faces as shown by the circled numbers in Figure 2. Positive pressures act into the element. Temperatures may be input as element body loads at the nodes.

PLANE45 is used for the 3-D modeling of solid structure, element PLANE45 is defined by eight node element and each element node is having three degree of freedom ,translation in $x,y,$ and z direction .The 3-D structure solid is of three types, hexahedron, tetrahedral and prism, in this study hexahedron elements have been selected for meshing. the critical regions have been meshed with fine and map mesh(structured mesh) to achieve accurate results.

3. Results and Discussion

The parameters used are shown in Table 1. To study the behavior of the device, the dimension of the device is varied according to previous research (Vivek et al., 2006; Lohit and Shiva, 2008; Heng Yang et al., 2005). The design is limited to a single beam cantilever structure and square proof mass. A comparative study is made for the analytical and FEM results of three models with different beam dimensions. The maximum displacement for the first model is shown in Figure 5 while Figures 6 to 11 show the deflection contours. The maximum displacement for the second model is shown in Figure 12 while Figures 13 to 18 show the deflection contours. The maximum displacement for the third model is shown in Figure 19 while Figures 20 to 22 show the deflection contours.

The maximum displacement linearly changed with the increase of acceleration for the first and second models but for the third model, the maximum displacement increased with the increase of acceleration up to $2g$ and then it decreased. Thus, the third model showed a low scale range than the other models. The second model displaced more than the first model with the same acceleration. Furthermore, the displacement of the second model exceeded the maximum distance between the electrodes, d_0 , up to $5g$. The same pattern was showed by the third model - the displacement exceeded the maximum distance between electrodes, d_0 , up to $1g$. Thus the first model showed better performance compared to the other models. In addition, it achieved a scale range of more than $6g$ because the displacement exceeded only at about $4.5\mu m$ for $6g$ acceleration but the distance between the electrodes, d_0 , was $19\mu m$.

4. Conclusions

The study on the design and the analysis of the capacitive micro cantilever beam accelerometer focusing on the deflection behavior is presented in the current paper. A comparative study is made between the analytical and FEM results according to the dimensions taken from the literature. ANSYS software is used to model, simulate and carry out FEM analysis. An analytical model is also simulated using C programming and the results obtained by FEM are in close agreement with the analytical results. The future scope for this work is performance analysis using system-level simulation techniques.

Acknowledgement

The authors would like to express sincere appreciation for the assistance of Mr. Mohd Kusairay Musa and Mr. Faisal Mohamad for their co-operation and assistance in providing support for the software. To Mr. Fazlan, Mr. Sanusi, Mr. Zamri and Puan Rohana, thanks for your kind help. Financial support from the Universiti Sains Malaysia Short Term Grant, 3004/PELECT/6035301 is gratefully acknowledged.

Nomenclature

- ρ : Specific mass
- E : Young Modulus
- b_l : Width of the beam
- a_l : Length of the beam
- h_l : Thickness of the beam

- b_2 : Width of the mass
 l : $a_2 - a_1$
 h_2 : Thickness of the mass
 a : Acceleration
 d_0 : Distance between electrodes
 F : Force

References

Ballestra, A., E. Brusa, M. Gh Munteanu, A. Soma. (2008). Experimental characterization of electrostatically actuated in-plane bending of microcantilevers. *Microsyst Technol.*, 14, 909–918.

DOI: 10.1007/s00542-008-0597-0

Bianco, S., M. Cocuzza, I. Ferrante, E. Giuri, C. F. Pirri, A. Ricci, L. Scaltrito, D. Bich, A. Merialdo, P. Schina and R. Correale. (2008). Silicon micro cantilevers with different actuation-readout schemes for absolute pressure measurement. *Journal of Physics: Conference Series*, 100, 1-4.

DOI:10.1088/1742-6596/100/9/092008

Chowdhury, S., M. Ahmadi and W.C. Miller. (2005). A closed-form model for the pull-in voltage of electrostatically actuated cantilever beams. *J. Micromech. Microeng.*, 15, 756–763.

DOI: 10.1088/0960-1317/15/4/012

Fricke, J. and E. Obermeier. (1993). Cantilever beam accelerometer based on surface micromachining technology, *J. Micromech. Microeng.*, 3, 190-192.

<http://iopscience.iop.org/0960-1317/3/4/005>

Heng Yang, Zhengyin Yu, Xinxin Li & Yuelin Wang. (2005). A Novel Pull-in Accelerometer Based on Cantilever Beam Mass Structure, *Sensors*, 2005 IEEE, 644-647.

DOI: 10.1109/ICSENS.2005.1597781

Lohit B.H. and Shiva Kumar. J. (2008). Analysis of micro capacitive accelerometer, Proceeding of International Conference on Microelectromechanical Systems (MEMS), (MEMS-08), Bhatkal India, CP16, 22-23 Oct. 2008.

Puersy, R. and S. Reyntjens. (1998). The characterization of a miniature silicon micromachined capacitive accelerometer. *J. Micromech. Microeng.*, 8, 127–133.

DOI: 10.1088/0960-1317/8/2/021

Vivek A., Tarun K. B. and Subhadeep B. (2006). Design steps for bulk micro machined single axis silicon capacitive accelerometer with optimised device dimensions, *Journal of Physics: Conference Series*, 34, 722–727.

DOI: 10.1088/1742-6596/34/1/119

Table 1. Parameters used

Geometry dimension	First model (μm)	Second model (μm)	Third model (μm)
Width of the beam, b_1	250	500	2
Length of the beam, a_1	700	500	50
Thickness of the beam, h_1	45	20	30
Width of the mass, b_2	2500	3000	20
Total length of the mass, $a_2 (l + a_1)$	3200	3500	500
Thickness of the mass, h_2	575	200	30
Distance between electrode, d_0	19	10	3
Mechanical properties			
Free space permittivity, ϵ_0	$8.8541878 \text{ E}^{-12}$	$8.8541878 \text{ E}^{-12}$	$8.8541878 \text{ E}^{-12}$
Young modulus, E	1.7 E^{11}	1.7 E^{11}	1.7 E^{11}
Specific mass of material, ρ	2230 kg/m^3	2230 kg/m^3	2230 kg/m^3

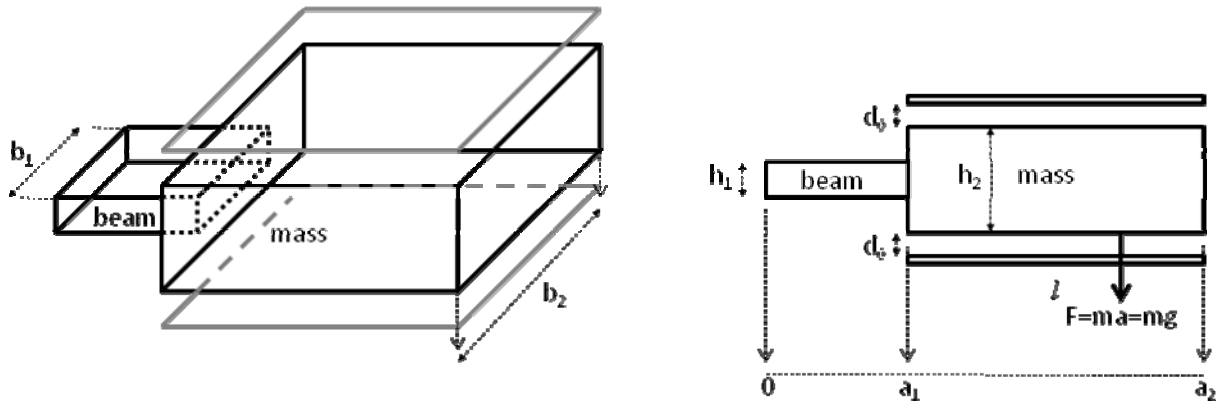


Figure 1. A simplified model for the cantilever beam-mass accelerometer

Figure 2. System interface for C programming

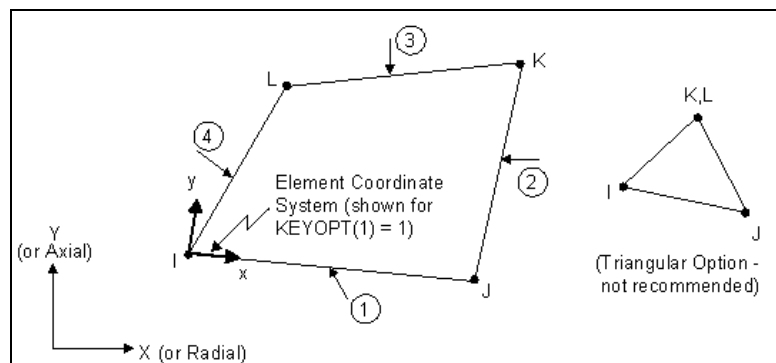


Figure 3. PLANE42 geometry

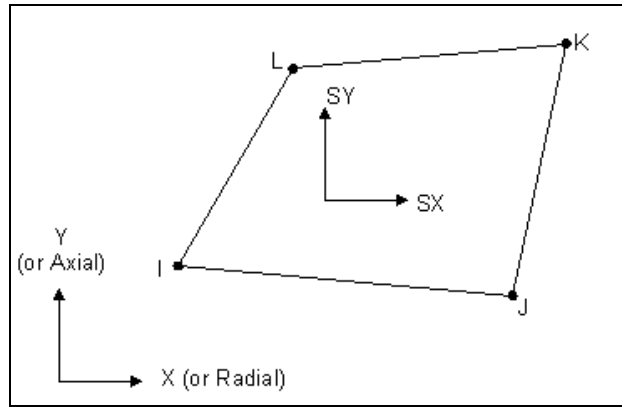


Figure 4. PLANE42 Output data

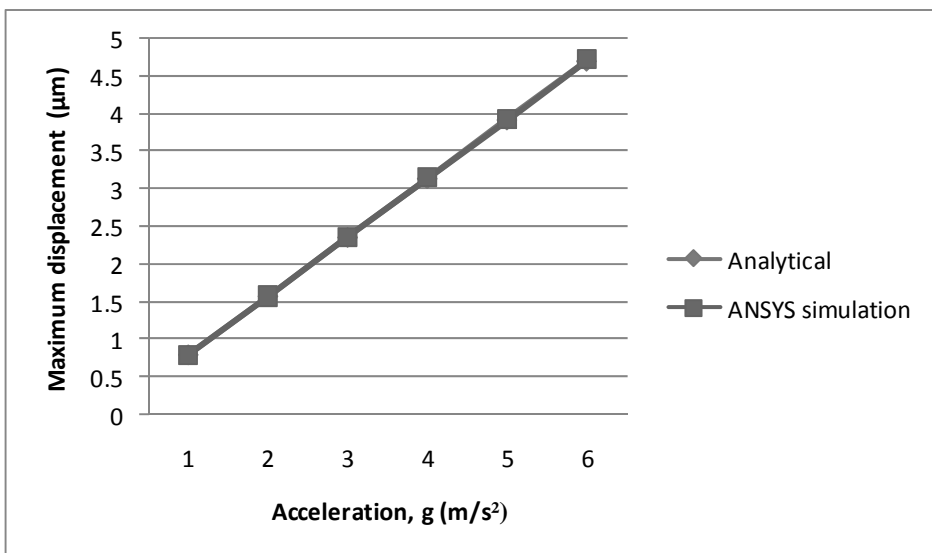


Figure 5. Maximum displacement with respect to applied acceleration for first model

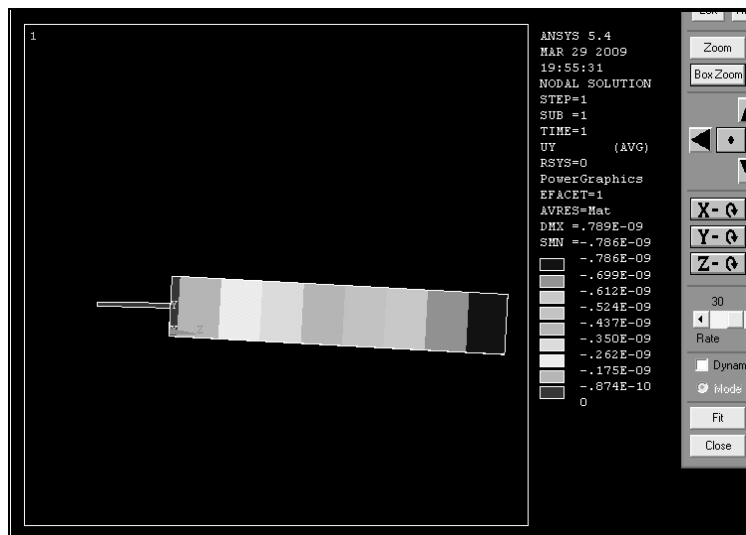


Figure 6. The maximum deflection for 1g

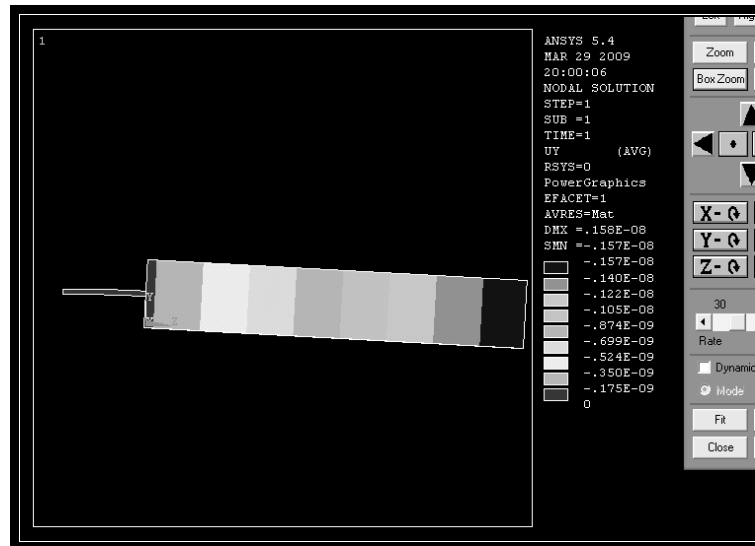


Figure 7. The maximum deflection for 2g

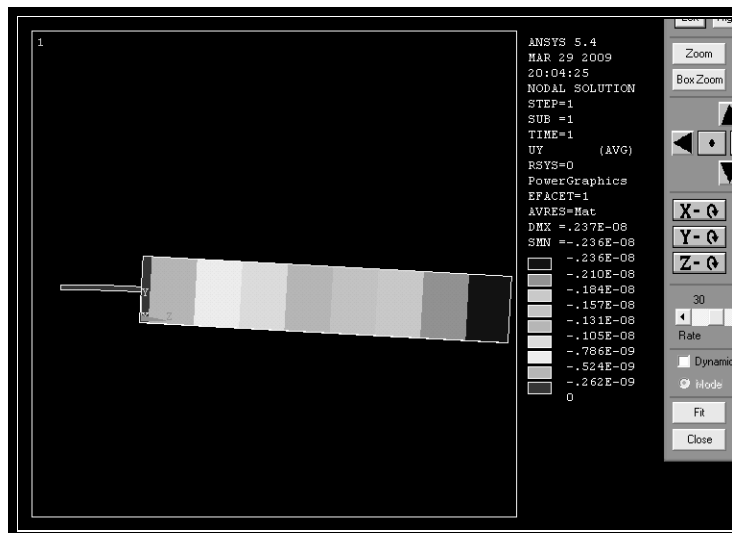


Figure 8. The maximum deflection for 3g

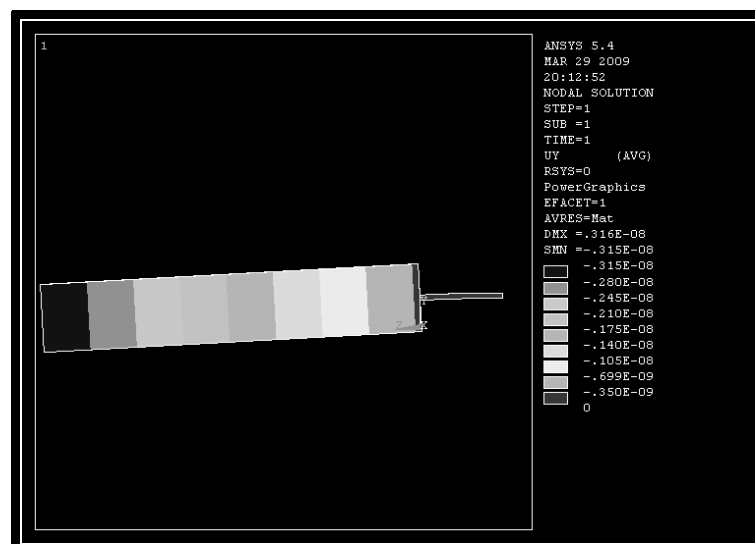


Figure 9. The maximum deflection for 4g

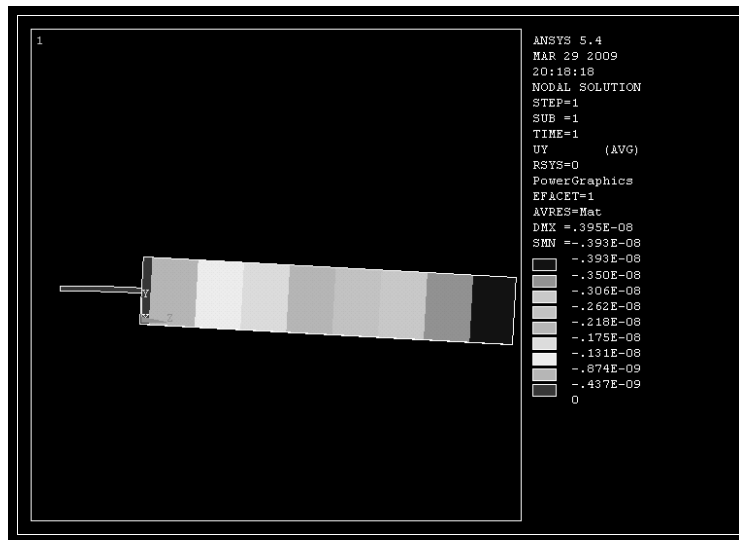


Figure 10. The maximum deflection for 5g

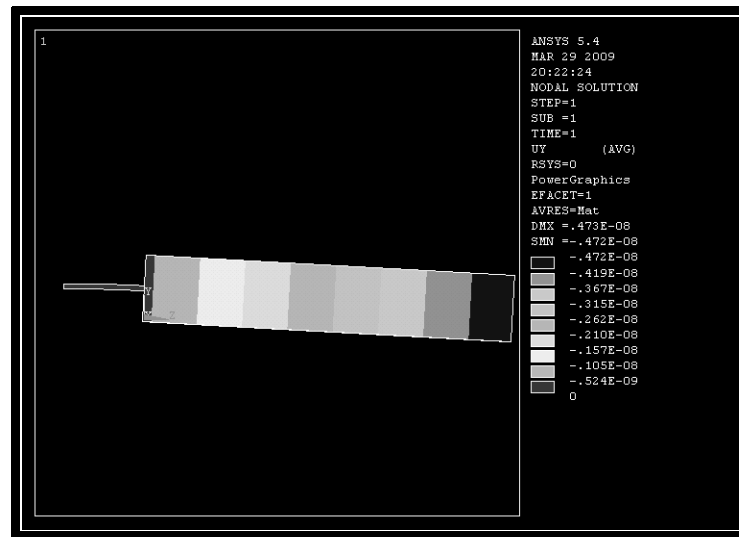


Figure 11. The maximum deflection for 6g

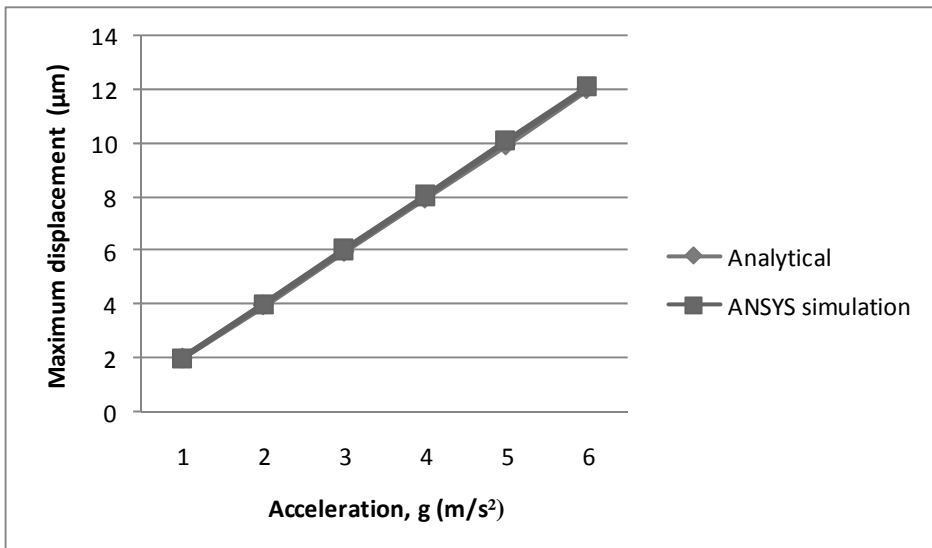


Figure 12. Maximum displacement with respect to applied acceleration for second model

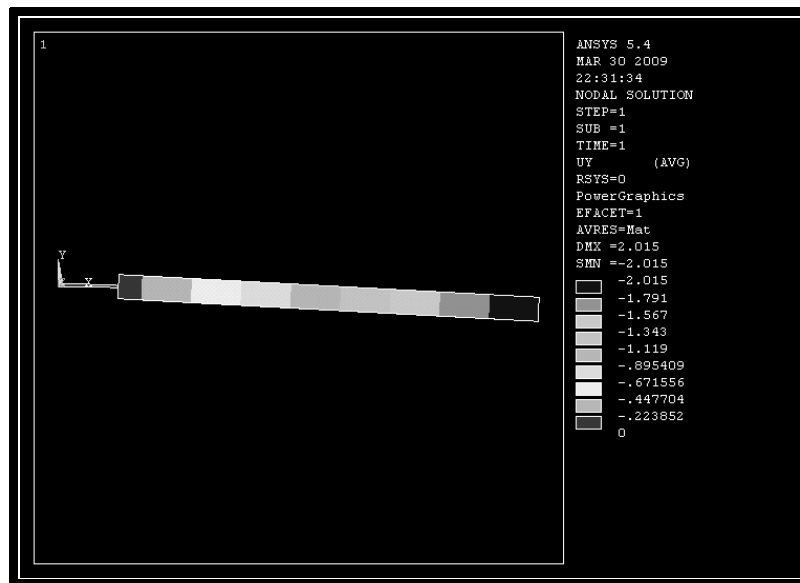


Figure 13. The maximum deflection for 1g

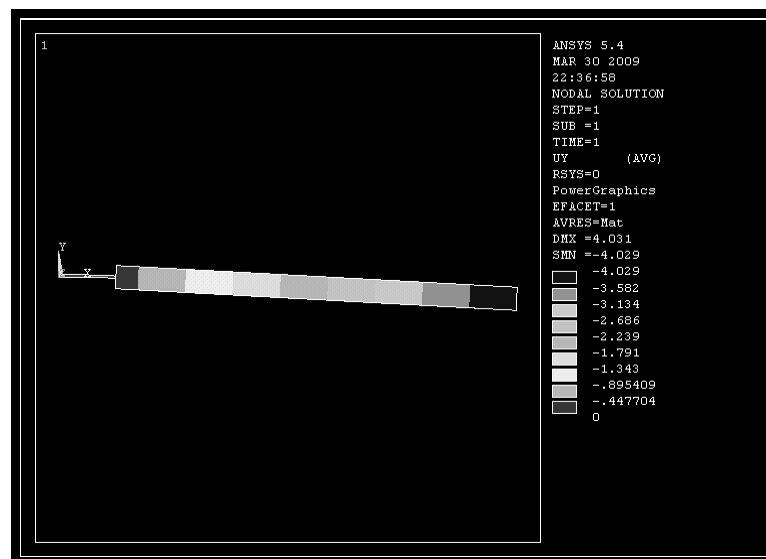


Figure 14. The maximum deflection for 2g

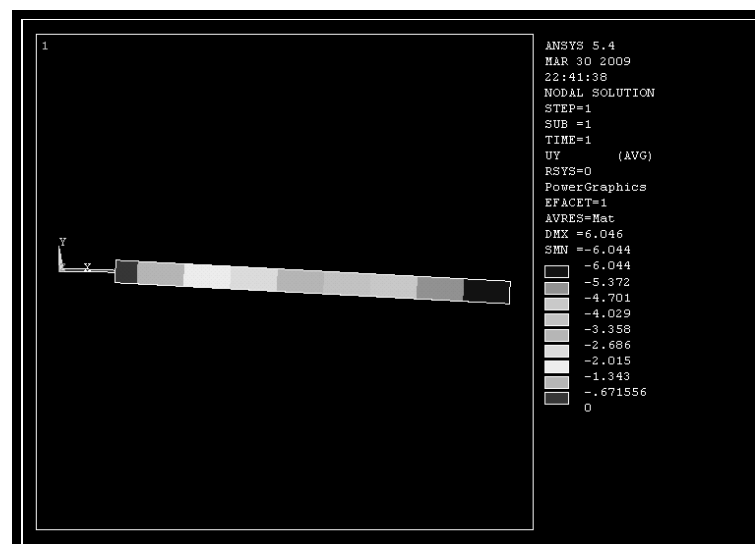


Figure 15. The maximum deflection for 3g

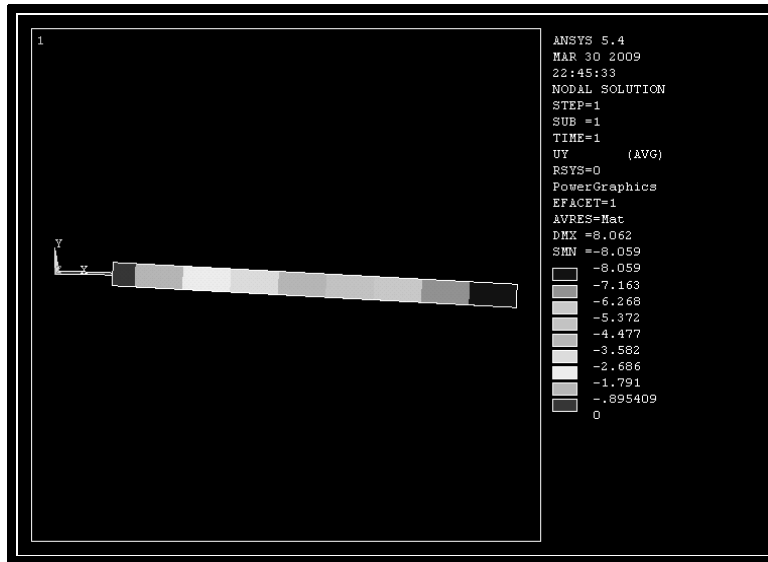


Figure 16. The maximum deflection for 4g

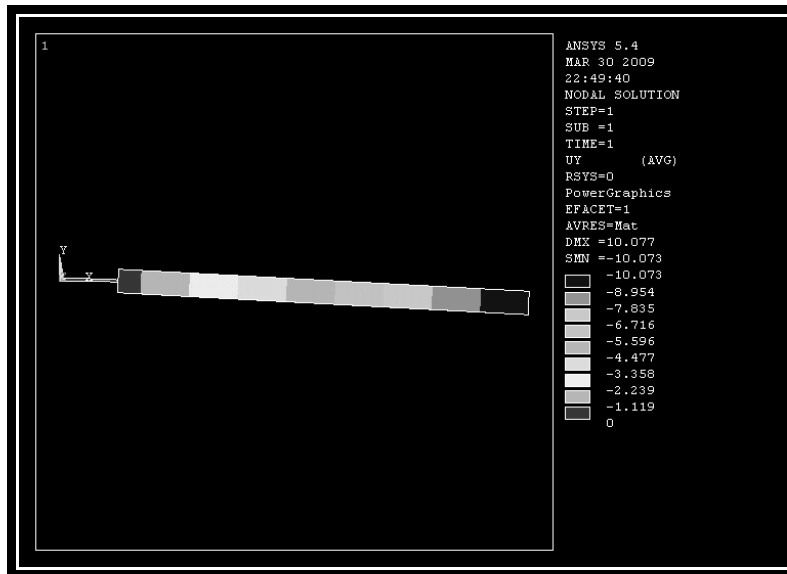


Figure 17. The maximum deflection for 5g

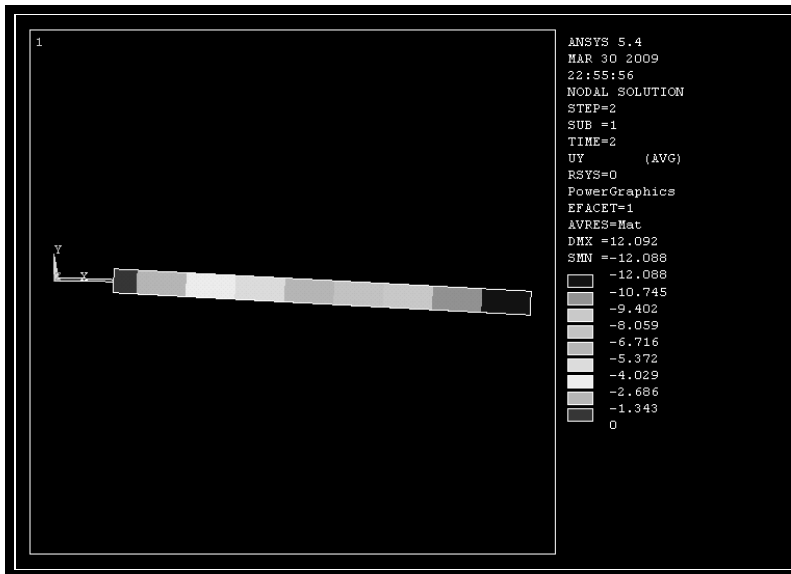


Figure 18. The maximum deflection for 6g

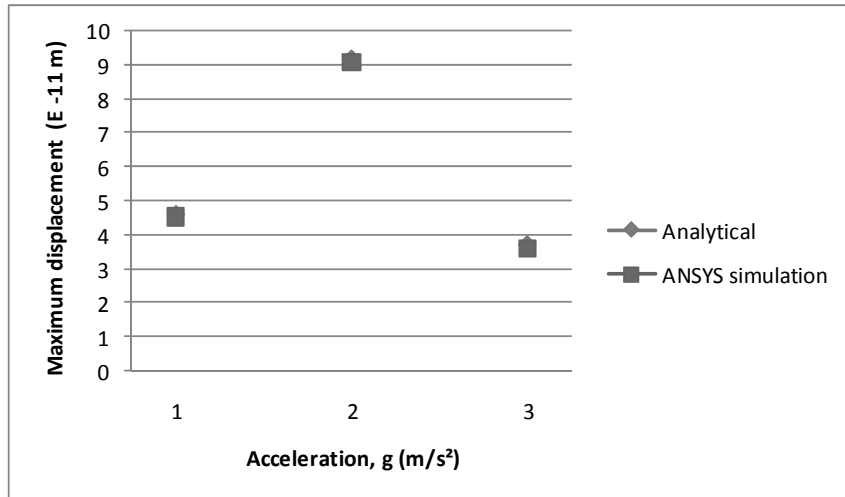


Figure 19. Maximum displacement with respect to applied acceleration for third model

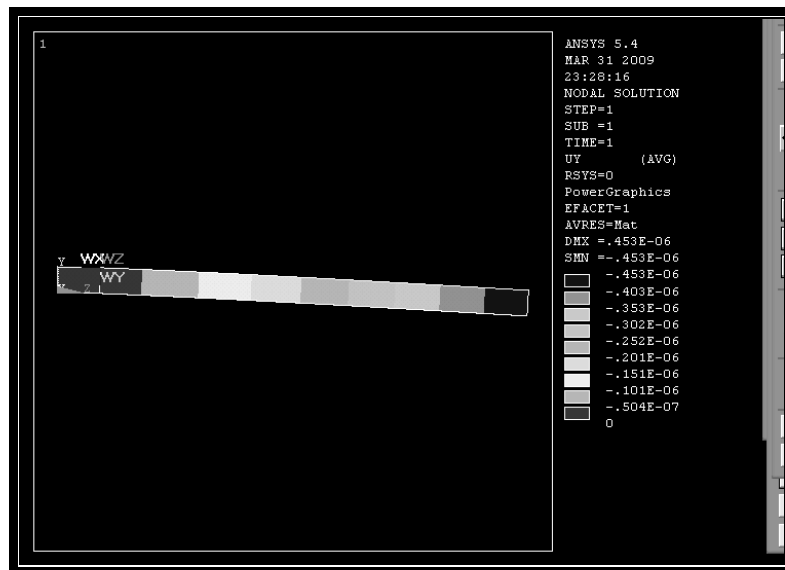


Figure 20. The maximum deflection for 1g

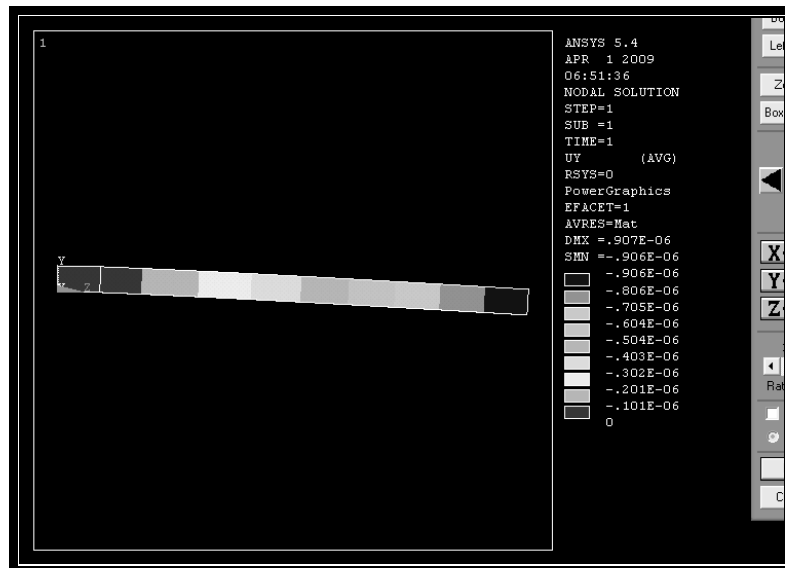


Figure 21. The maximum deflection for 2g

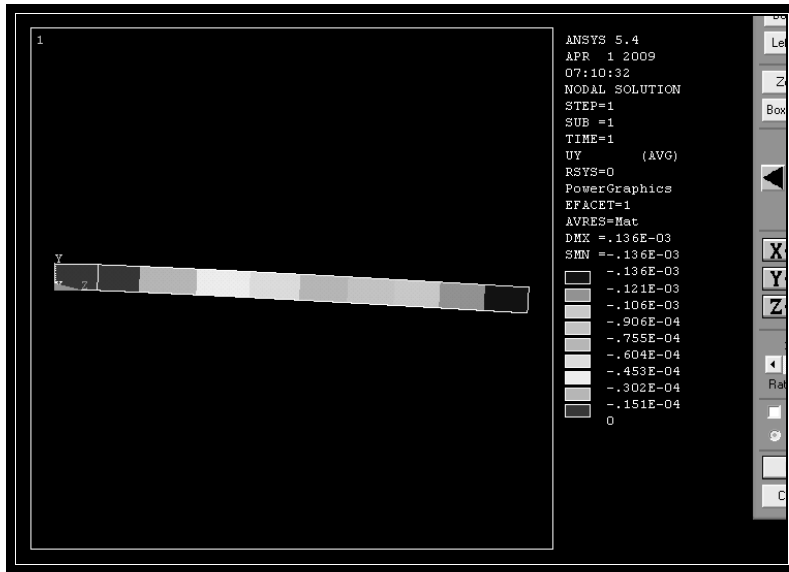


Figure 22. The maximum deflection for 3g